Analysis of the Absorption and Magnetic Circular Dichroism Spectra of Low Spin ($S = {}^1/_2$) Iron(III) Phthalocyanine

Edward A. Ough and Martin J. Stillman*

Department of Chemistry, The University of Western Ontario, London, Ontario, N6A 5B7 Canada

Received May 10, 1994[⊗]

Absorption and magnetic circular dichroism (MCD) spectra are reported for metal oxidized bis(cyano)iron(III) phthalocyanine ($Na[(CN)_2Fe^{III}Pc(-2)]$). Low temperature (<4 K) MCD spectra are used to determine the Lande g factor and the ground state spin and orbital degeneracy in $Na[(CN)_2Fe^{III}Pc(-2)]$. Analysis of the low temperature, variable field MCD spectra for $Na[(CN)_2Fe^{III}Pc(-2)]$ allow the assignment of the ground state as ^2E_g. The orbital degeneracy in the ground state required low temperature absorption and MCD spectra for spectral deconvolution calculations. The fits reported here for $Na[(CN)_2Fe^{III}Pc(-2)]$ represent the first comprehensive spectral analysis of an open shell metallophthalocyanine with an orbitally degenerate ground state. Ring $\pi \rightarrow \pi^*$ (Q, B1, B2, N, and L) transitions, $e_g(d\pi) \rightarrow 1b_{1u}(\pi),1b_{2u}(\pi)$ metal to ligand charge transfer (LMCT) transitions, and a series of ligand to metal charge transfer (LMCT) transitions into the ${}^3/_4$-filled iron(III) $e_g(d\pi)$ orbitals $[\{a_{iu}(\pi),b_{iu}(\pi)\} \rightarrow e_g(d\pi)$ $(i = 1,2)]$ are identified in the optical spectra of $Na[(CN)_2Fe^{III}Pc(-2)]$. Individual electronic transitions (with assignments) are located at 780 (LMCT2); 686 (Q); 645 (LMCT3); 613, 601, 550, and 541 (MLCT1); 513 (LMCT4); 445, 429, 407, and 394 (MLCT2); 346 (B1); 298 (LMCT5); 317 (B2); 273 (N); and 260 nm (L).

Introduction

The number of metal oxidation states (I to IV) available in iron phthalocyanine (FePc)[1-3] makes it an ideal molecule to study when developing artificial systems that mimic biological molecules for which redox chemistry plays a major role, for example, the cytochromes, the peroxidases, and the catalases. The Fe(II)/Fe(III) oxidation couple in FePc, a value that is vital to electron transfer in the cytochromes within the electron transfer pathway, ranges from −0.20 to +0.80 V in a variety of axially ligated $(L)_2FePc$ complexes.[3] The "tunability" of this couple is achieved by changing either the solvent or the axial ligand and makes the $(L)_2FePc$ species ideal for use in electronic devices that operate at the molecular level. The variability of this redox couple and the greater thermal and chemical stability of the phthalocyanines, compared to the parent porphyrins, make the FePc molecule an attractive candidate for use in molecular devices.

In a paper by Lever et al.[4] the potential of the Fe(II)/Fe(III) couple was related to the energy of charge transfer (CT) bands in the electronic spectrum. Although this study did not take into account the effect of configuration interaction,[5,6] it did provide a convenient starting point for groups attempting a more comprehensive analysis. Previous studies on closed shell metallophthalocyanines[1,7-11] demonstrate the value of coupling together analysis of the absorption and magnetic circular dichroism (MCD) spectra to identify the energies, widths and intensities of individual bands, which then allows determination of the origins of the observed transitions. In this present paper, we report the first detailed analysis of the optical spectrum of low spin ($S = {}^1/_2$) $(L)_2Fe^{III}Pc$. From an analysis of the low temperature absorption and MCD spectra of sodium bis(cyano)-iron(III) phthalocyanine using spectral deconvolution techniques, we determine the degeneracy of the ground state and estimate the orbital g factor.

Experimental Section

Materials and Methods. $Fe^{II}Pc(-2)$ (Kodak) was purified by repeated (three times) vacuum sublimation. The fragmentation pattern in the mass spectrum of purified $Fe^{II}Pc(-2)$ was checked to ensure that there was no modification of the peripherally fused benzene rings. Sodium cyanide (NaCN; Fisher), 1,1-dichloromethane (DCM; BDH), *N*,*N*-dimethylformamide (DMF; BDH) and bromine (Br_2; BDH) were used without further purification. 1-Chlorobutane (CB; BDH) was double distilled prior to its use.

$Na[(CN)_2Fe^{III}Pc(-2)$ was prepared by oxidizing $Na_2[(CN)_2Fe^{II}Pc(-2)]$, which was prepared according to literature methods,[10,12] with 0.001 M Br_2 in DCM. Absorption spectra were measured during the stepwise titration to follow the oxidation from $Na_2[(CN)_2Fe^{II}Pc(-2)]$ to $Na[(CN)_2Fe^{III}Pc(-2)]$. The oxidation titrations were repeated in triplicate to ensure that the results obtained were reproducible.

Spectroscopic Methods. All room temperature spectra were recorded from nitrogen saturated DCM solutions. Spectra were measured in 1 cm path length square UV cells or 1 cm path length cylindrical MCD cells. Low temperature absorption and MCD spectra

* To whom correspondence should be addressed: tel., (519) 661-3821; FAX, (519) 661-3022; Internet, STILLMAN@UWO.CA.

⊗ Abstract published in *Advance ACS Abstracts,* July 1, 1995.

(1) Stillman, M. J.; Nyokong, T. In *Phthalocyanines: Properties and Applications*; Leznoff, C. C., Lever, A. B. P., Eds., VCH Publications: New York, 1989; Vol. 1, Chapter 4, pp 133–289.
(2) Stillman, M. J. In *Phthalocyanines: Properties and Applications*; Leznoff, C. C., Lever, A. B. P., Eds., VCH Publications: New York, 1992; Vol. 3, Chapter 5, pp 227–296.
(3) Lever, A. B. P.; Milaeva, E. R.; Speier, G. In *Phthalocyanines: Principles and Applications*; Leznoff, C. C., Lever, A. B. P., Eds., VCH Publications: New York; 1992, Vol. 3, Chapter 1, pp 1–69.
(4) Lever, A. B. P.; Pickens, S. R.; Minor, P. C.; Licoccia, S.; Ramaswany, B. S.; Magnell, K. *J. Am. Chem. Soc.* **1981**, *103*, 6800–6806.
(5) Gouterman, M. Physical Chemistry. In *The Porphyrins*; Dolphin, D., Ed.; Academic Press: New York, 1989; Vol. III, Part A, pp 1–165.
(6) McHugh A. J.; Gouterman, M.; Weiss, C. *Theor. Chim. Acta* **1972**, *24*, 346.
(7) Nyokong, T.; Gasyna, Z.; Stillman, M. J. *Inorg. Chem.* **1987**, *26*, 1087–1095.
(8) Ough, E. A.; Nyokong, T.; Creber, K. A. M.; Stillman, M. J. *Inorg. Chem.* **1988**, *27*, 2725–2732.
(9) Ough, E. A.; Gasyna, Z.; Stillman, M. J. *Inorg. Chem.* **1991**, *30*, 2301–2310.
(10) Nyokong, T. N. Ph.D. Thesis, The University of Western Ontario, London, Ontario, Canada, 1986.
(11) Nyokong, T.; Gasyna, Z.; Stillman, M. J. *Inorg. Chem.* **1987**, *26*, 548–553.
(12) Martin, K. A. M. M.Sc. Thesis, The University of Western Ontario, London, Ontario, Canada, 1979.

0020-1669/95/1334-4317$09.00/0

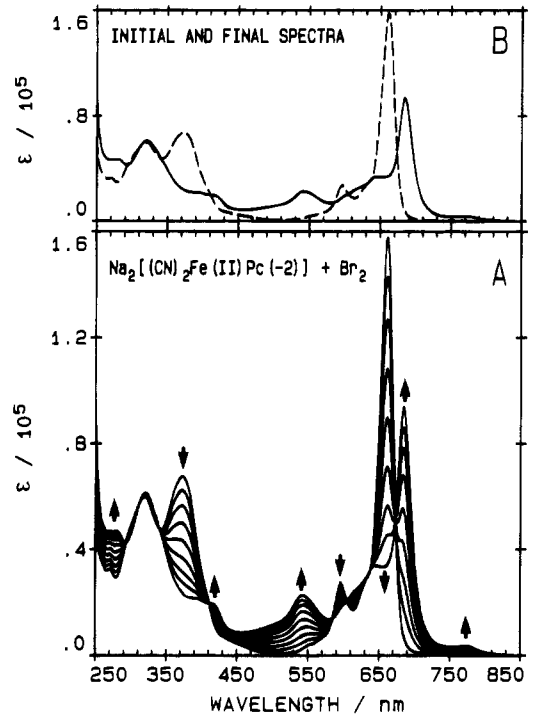

Figure 1. (A) Absorption changes observed during the chemical (Br_2) oxidation of $Na_2[(CN)_2Fe^{II}Pc(-2)]$ dissolved in 98:2 DCM:DMF to $Na[(CN)_2Fe^{III}Pc(-2)]$. (B) Initial (– – –) and final (—) absorption spectra recorded during the titration of Br_2 into $Na_2[(CN)_2Fe^{II}Pc(-2)]$.

were measured on glassed samples prepared in 70:30 mixtures of DCM and CB. Absorption spectra were recorded on a Cary Model 2200 spectrophotometer controlled by an IBM S9001 computer using the computer program CARYSCAN.[13] For the low temperature absorption measurements, the spectra were measured on samples placed inside an Oxford Instruments CF-204 cryostat. MCD spectra were recorded at room temperature using a Jasco J500C spectropolarimeter controlled by an IBM S9001 computer using the computer program CD-SCAN5,[14,15] with a field of 5.5 T provided by an Oxford Instruments SM2 superconducting magnet. Calibration of the MCD signal intensity was performed using an aqueous solution of cobalt(II) sulphate, with the negative band intensity at 510 nm, as $\Delta\epsilon_M = -1.9 \times 10^{-2}$ L mol^{-1} cm^{-1} T^{-1}. Low temperature MCD spectra were measured from samples placed in an Oxford Instruments SM4 superconducting magnet which has a maximum field strength of 5 T.

Data Analysis. As with our previous work, Gaussian band shapes were used to fit the absorption and MCD spectra. Fitting was performed by the use of the program SIMPFIT,[16] which utilizes a Simplex routine, to fit the MCD spectra and a least-squares minimization routine based on second derivatives to fit the absorption data. The database management program Spectra Manager[17] was used to manipulate the spectral data.

Results

Chemical Oxidation of Iron(II) Phthalocyanine. Absorption spectral changes observed during the titration of 0.001 M Br_2 into a solution of $Na_2[(CN)_2Fe^{II}Pc(-2)]$ are plotted in Figure 1. A number of significant spectral changes are observed during oxidation. (1) The Q band maximum shifts from 660 to 685 nm and exhibits a 30% reduction in intensity. (2) New bands assigned as charge transfer appear to the low energy (700–850 nm) side of the Q band and overlap the vibrational components (Q_{vib}) of the Q band between 550 and 670 nm. (3) The 380 nm band in the $Na_2[(CN)_2Fe^{II}Pc(-2)]$ spectrum is lost. The presence of sharp isosbestic points near 410, 585, 600, and 670 nm indicates that oxidation proceeds cleanly without any side reactions occurring. The absence of the 500 nm marker band indicative of ring oxidation[2] verifies that the site of oxidation is the metal. On the basis of published absorption spectra for iron(III) phthalocyanines,[1,2,18] the oxidation product is determined to be $Na[(CN)_2Fe^{III}Pc(-2)]$.

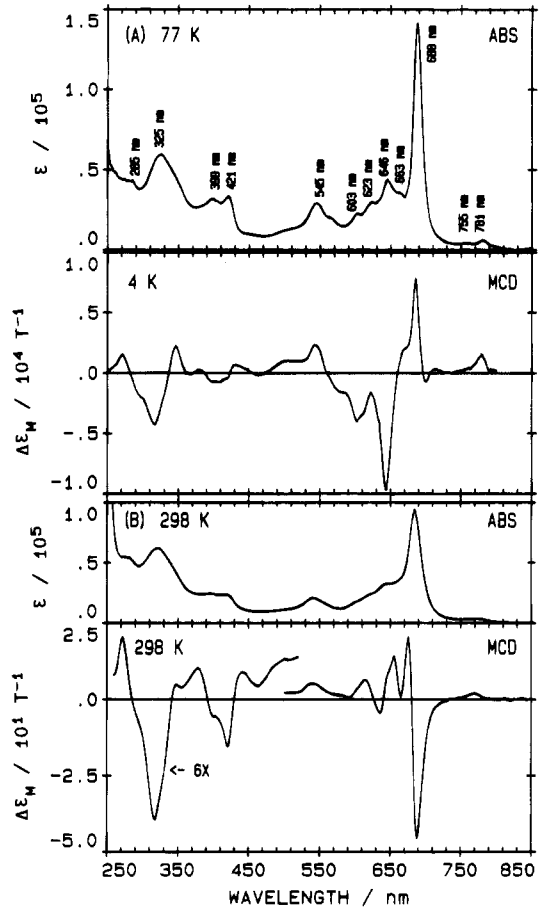

Figure 2. (A) 77 K absorption (ABS) and 4 K MCD (4 K) spectra for a 1 mm glass of $Na[(CN)_2Fe^{III}Pc(-2)]$ and (B) 298 K absorption and MCD spectra for $Na[(CN)_2Fe^{III}Pc(-2)]$ in DCM (ϵ for the Q_{00} transition (λ_{max} = 684 nm) is 93 800 L mol^{-1} cm^{-1} at 298 K and 141 500 L mol^{-1} cm^{-1} at 77 K). Band maxima are shown at 285, 325, 399, 421, 545, 603, 623, 646, 663, 688, 755, and 781 nm.

Room Temperature and Low Temperature Absorption and MCD Spectra. Both the absorption and MCD spectra of $Na[(CN)_2Fe^{III}Pc(-2)]$ exhibit significant temperature dependencies between room temperature and 4 K, as seen in Figure 2. These effects are best seen for the Q band at 680 nm where the absorption spectral intensity increases 50% and the band width decreases 30%. The temperature effects observed in the absorption spectrum arise mainly from the depopulation of thermally excited vibronic states. The spectrum at 77 K (Figure 2A) sharpens considerably to show many more resolved bands than at room temperature (Figure 2B). Compared with the absorption spectrum of main group phthalocyanines, for example ZnPc and MgPc,[1] the spectrum at 77 K is very much more complicated, with bands located throughout the near-UV and visible regions and into the near-IR region. Overlaying the Q, B, N, and L bands expected for the $\pi-\pi^*$ transitions are both metal to ligand charge transfer (MLCT) and ligand to metal charge transfer (LMCT) bands.[1]

(13) Ough, E. A.; Stillman, M. J. *Inorg. Chem.* **1994**, *33*, 573–583.
(14) Gasyna, Z.; Browett, W. R.; Nyokong, T.; Kitchenham, R.; Stillman, M. J. *Chemom. Intell. Lab. Syst.* **1989**, *5*, 233–246.
(15) Mack, J.; Stillman, M. J. To be published.
(16) Browett, W. R.; Stillman, M. J. *Comput. Chem.* **1987**, *11*, 241–250.
(17) Browett, W. R.; Stillman, M. J. *Comput. Chem.* **1987**, *11*, 73–82.
(18) Stillman, M. J.; Thomson, A. J. *J. Chem. Soc., Faraday Trans. 2* **1974**, *70*, 790–804.

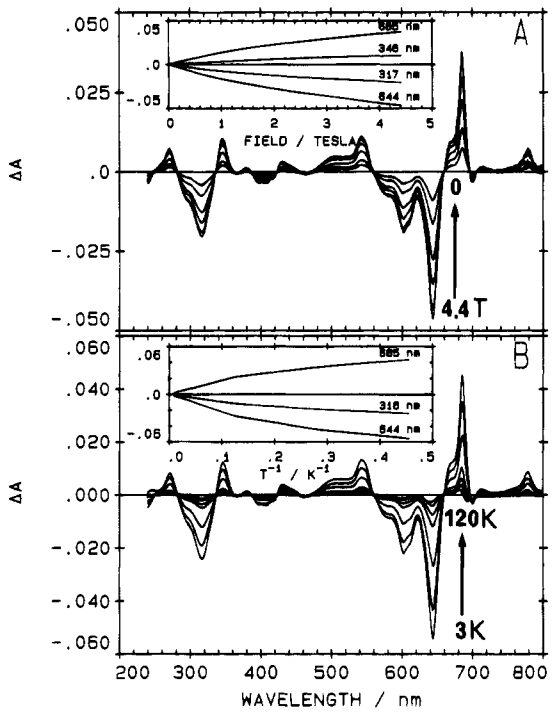

Figure 3. MCD changes observed for a 1 mm glass of $Na[(CN)_2Fe^{III}Pc(-2)]$ (A) when the temperature is held constant at 3.8 K and the magnetic field is varied between 0 and 4.4 T (the inset displays the change in MCD intensity versus magnetic field at four wavelengths) and (B) when the temperature is varied between 3 and 120 K under a constant 3.92 T magnetic field (the inset displays the change in MCD intensity versus temperature at three wavelengths). The arrows show the change in MCD spectral intensity for the negatively-signed band at 644 nm as a function of field (A) or temperature (B).

Much more dramatic effects are observed when the MCD spectrum is recorded at 4 K (Figure 2). Because the ground state is orbitally degenerate, intense C terms dominate the MCD spectrum (the signal intensity is approximately 100 times that at room temperature). Similar effects are also found for iron(III) porphyrins[20] and the low spin ferric heme proteins where the MCD spectra are dominated by temperature dependent C terms.

Low Temperature MCD Spectra. The MCD spectrum of $Na[(CN)_2Fe^{III}Pc(-2)]$ is highly field and temperature dependent. The spectrum recorded at 3.8 K is plotted in Figure 3A for magnetic flux densities between 0 and 4.4 T. Inspection of the negative and positive intensity of the bands at 644 and 685 nm indicates that ΔA is not linear with respect to the magnetic field intensity and saturates (approaches a local maximum or minimum value) at high applied magnetic fields. The inset in Figure 3A displays the saturation behavior at 317, 346, 644, and 685 nm. The same behavior occurs when the magnetic field is held constant at 3.92 T and the sample temperature is varied between 3 and 120 K (Figure 3B). ΔA at the three wavelengths 316, 644, and 685 nm approaches asymptotic values as the temperature falls below 4.2 K (the inset in Figure 3B). Saturation of the MCD signal in the temperature and field dependence plots for $Na[(CN)_2Fe^{III}Pc(-2)]$ indicates that population of the upper component of the orbitally degenerate ground state has been reduced to zero.

The appearance of a strongly temperature dependent MCD signal unambiguously identifies a degenerate ground state.[19] Because the MCD signal is proportional to $(B + C/kT)$ a plot

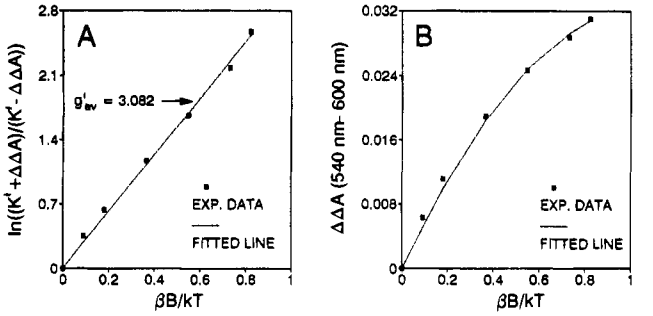

Figure 4. Plots of (A) $\ln[(K' + \Delta\Delta A)/(K' - \Delta\Delta A)]$ versus $\beta\mathbf{B}/kT$ and (B) $\Delta\Delta A$ versus $\beta\mathbf{B}/kT$, which present the experimental and fitted data obtained for a 3.6 K glassed sample of $Na[(CN)_2Fe^{III}Pc(-2)]$. $\Delta\Delta A$ represents the MCD spectral intensity difference between the 540 and 600 nm MCD bands and K' is the intensity of $\Delta\Delta A$ when the MCD signal is saturated. See the text for explanation of K' and g_{av}'.

of ΔA vs $1/kT$ will yield the fraction of C term intensity in the MCD signal. Clearly, the minimal deviation from linearity observed in Figure 4A indicates that only a small contribution from temperature-independent B terms is present.[36] Considering options for the ground state, we can conclude that the ground state is orbitally degenerate, and, in the absence of significant EPR signals, the ^2E state expected for low spin Fe(III) is present as proposed previously by Kennedy et al. (vide infra).[22]

Determination of the Lande g Factor. The strong dependence of the MCD signal on the magnetic field induction, B shown in Figure 3A and the strong dependence of the MCD signal on temperature shown in Figure 3B together allow an estimate to be made of the g_{av} for the ground state. Extraction of ground state magnetic moment data from MCD spectral data measured as a function of both temperature and field has been used for a number of systems. For the low spin Fe(III) in $Na[(CN)_2Fe^{III}Pc(-2)]$ we anticipate a Kramers doublet as shown in Figure 8. The relative population of a Zeeman split Kramer doublet depends on the Boltzman distribution function ($N_A/N_B = \exp[-\Delta E/kT]$).[19] The magnetic field strength ($\mathbf{B}$), the Bohr magneton (β) and the averaged orbital g factor (g_{av}) determine the energy separation ($\Delta E = g_{av}\beta\mathbf{B}$) between the two energy levels within the doublet. If the MCD signal saturates (this occurs when there is 100% population of the lower energy level in the ground state Kramers doublet) then the spectral intensity (ΔA) at a specific wavelength can be plotted against $\beta\mathbf{B}/kT$ and the equation $\Delta A = K \tanh(g_{av}\beta\mathbf{B}\cos(\Theta)/2kT)$, which is adapted from ref 19, can be used to determine g_{av}. In this equation, the unknown variable K represents ΔA at saturation, a value independent of the g_{av}, and Θ is the angle between the x/y plane and the direction of the magnetic field (which for the MCD experiment is the direction of the light beam). In the absence of values for K and Θ, solution of this equation cannot be obtained analytically; however, by rearrangement and use of iterative procedures, values for K and g_{av} can be estimated. First, though we must address the problem of orientation of the planar metallated phthalocyanine. The $Fe^{III}Pc(-2)$ exists in a random orientation in the frozen solution. Integration of Θ, the angle between the x/y plane and the optic axis, can provide the reduction factor experienced by the randomly oriented planar molecules.

Therefore, we can estimate ΔA from $\int K\cos(\Theta)\tanh(g_{av}\beta\mathbf{B}\cos(\Theta)/2kT$. Integration leads to $\Delta A = (K/2)\tanh(1.5g_{av}\beta\mathbf{B}/2kT)$, and by setting $K' = K/2$ and $g'_{av} = 2g_{av}/3$, we obtain $\Delta A = K'\tanh(g'_{av}\beta\mathbf{B}/2kT)$.

(19) Piepho, S. B.; Schatz, P. N. *Group Theory in Spectroscopy, with Applications to Magnetic Circular Dichroism*; John Wiley and Sons: New York, 1983.

(20) Sharonov, Y.A. Physicochemical Biology Review. In *Soviet Scientific Reviews*; Skulachev, V. P., Ed.; Harwood Academic Publishers: New York, 1991; Section D, Vol. 10(3).

Alternative approaches to the solution of this equation involve plotting families of curves for a range of values of g_{av} as a function of either temperature or applied magnetic field. In our analysis we plotted the experimental data as a function of ΔA vs $\beta\mathbf{B}\cos(\Theta)/2kT$ and this experimental line was fitted in an attempt to obtain an estimate of g_{av}. Figure 4 shows the lines obtained following this latter approach for $Fe^{III}Pc$ using the MCD data shown in Figure 3.

The MCD signal for $Na[(CN)_2Fe^{III}Pc(-2)]$ did not saturate under the lowest temperatures (<2 K) and the strongest magnetic fields (>4.5 T) available. Without a definite value for K, fitting the ΔA versus $\beta\mathbf{B}/kT$ plot will yield an infinite number of values for g_{av}. This problem can be alleviated by rearranging the hyperbolic tangent equation to the linear equation: $\ln[(K' + \Delta A)/(K' - \Delta A)] = g_{av}'\beta\mathbf{B}/kT$. A least squares routine can be employed to determine unique values for K' and g_{av}' from a $\ln[(K' + \Delta A)/K' - \Delta A)]$ versus $\beta\mathbf{B}$/kT plot. The difference (χ^2) between the experimental data and a line of best fit was minimized in the determination of g_{av}'. The $\ln[(K' + \Delta\Delta A)/(K' - \Delta\Delta A)]$ versus $\beta\mathbf{B}/kT$ plot for $Na[(CN)_2Fe^{III}Pc(-2)]$ in Figure 4A approaches linearity when $K' = (3.61 \pm 0.06) \times 10^{-2}$ and $g_{av}' = 3.08 \pm 0.04$. $\Delta\Delta A$ is the difference in the MCD spectral intensity between the bands at 540 and 600 nm. Using the intensity difference between two close lying, oppositely signed MCD bands ensures that base line distoriton effects introduced by strains in the glass are minimized. The K' and g_{av}' values for $Na[(CN)_2Fe^{III}Pc(-2)]$ are inserted into the hyperbolic tangent equation, and the resulting curve is plotted in Figure 4B to demonstrate the accuracy of the K' and g_{av}' values. A value of $g'_{av} = 3.08$ gives $g_{av} = 3.08 \times {}^3/_2 = 4.6$. The increase in the value of g_{av} is intuitively expected as the effect of the tumbling will be to reduce the measured magnitude of the MCD C terms.

Spectral Band Deconvolution Calculations. Since the ground state of $Na[(CN)_2Fe^{III}Pc(-2)]$ is orbitally degenerate, the resolved MCD C terms observed at low temperatures must be used for spectral band deconvolution calculations. At 4 K in a 4.41 T magnetic field, the Zeeman split low energy component of the ground state Kramers doublet is 93% occupied. Depopulation of the higher energy component ensures that the observed nonderivative Gaussian band shapes provide reliable band widths and band centers for the electronic transitions contributing to the MCD spectrum. Because our deconvolution calculations assume the rigid shift approximation,[19] the MCD spectra are scaled so that the MCD spectral intensity ($\Delta\epsilon$) is linear with respect to the applied magnetic field. The use of 77 K absorption spectra ensures that spectral intensity due to vibronic hot bands is minimized.

The 77 K absorption and 4 K MCD fit for the Q (500−800 nm) and B (250−500 nm) regions of $Na[(CN)_2Fe^{III}Fc(-2)]$ are displayed in Figures 5 and 6. The lack of systematic noise in the MCD residuals shown in Figures 5 and 6 suggests that the bands used in the fits reliably reproduce the numbers and the positions of electronic transitions that comprise the electronic spectra. Because of the degeneracy of the ground state in $Na[(CN)_2Fe^{III}Pc(-2)]$, absorption bands are fit to nonderivative C terms in the MCD spectra. The fitting parameters obtained for the Q and B regions of $Na[(CN)_2Fe^{III}Pc(-2)]$ are listed in Table 1.

Discussion

Royal blue $L(X)Fe^{III}Pc(-2)$ can be obtained by chemical[21−25] and electrochemical[10] oxidation of $L_2Fe^{II}Pc(-2)$, and by addition

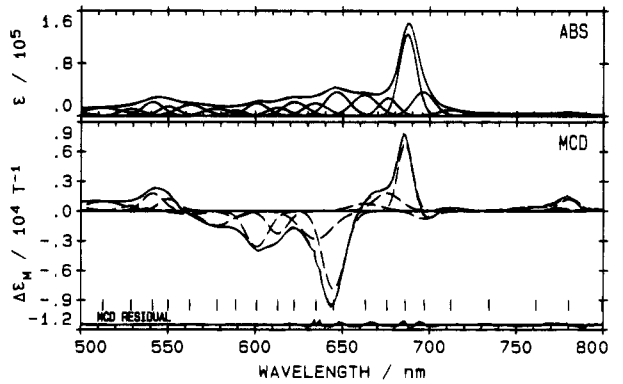

Figure 5. Results of a band analysis on the 77 K absorption and 4 K MCD spectra for 1 mm glasses of $Na[(CN)_2Fe^{III}Pc(-2)]$ in the visible region (bands 1−24). (a) Absorption: (—) experimental data; (− − −) fitted data; (—) individual bands. (b) MCD: (—) experimental data; (− − −) fitted data; (− −) individual bands.

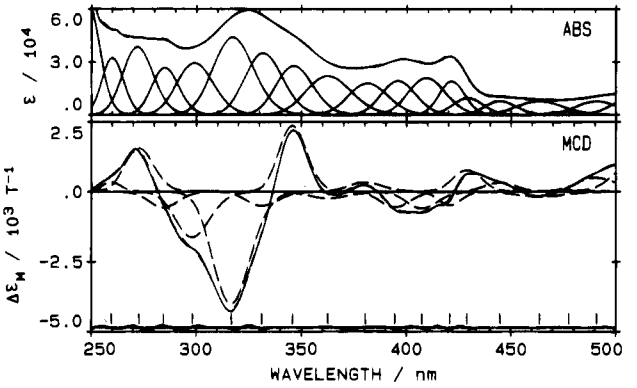

Figure 6. Results of a band analysis of the 77 K absorption and 4 K MCD spectra for 1 mm glasses of $Na[(CN)_2Fe^{III}Pc(-2)]$ in the ultraviolet region (bands 25−44). (a) Absorption: (—) experimental data; (− − −) fitted data; (—) individual bands. (b) MCD: (—) experimental data; (− − −) fitted data; (− −) individual bands.

of basic ligands to the intermediate spin $(Cl)Fe^{III}Pc(-2)$ complex.[25,26] In his review of the electrochemical properties of metallophthalocyanines, Lever[3] lists $E_{1/2}(Fe(II)/Fe(III))$ values for a series of $L_2Fe^{II}Pc(-2)$ complexes and a variety of counterions. The 1.0 V variability in $E_{1/2}$ can be explained by studying the Nicholson−Shain (NS) plots for $L_2Fe^{II}Pc(-2)$.[3,24,27,28] Analysis of the NS plots indicates that metal oxidation (eq 1) is followed by ligand exchange (eq 2). The π donor−π acceptor properties of the axial ligands influence the ease of oxidation, while the iron(III) oxidation state is stabilized by axial ligation of a counterion.

$$L_2Fe^{III}Pc(-2) \rightleftharpoons [L_2Fe^{III}Pc(-2)]^+ + e^- \quad (1)$$

$$[L_2Fe^{III}Pc(-2)]^+ + X^- \rightleftharpoons L(X)Fe^{III}Pc(-2) + L \quad (2)$$

The negatively charged couter ion (X^-) which is positioned *trans* to a basic ligand (L) stabilizes the iron(III) oxidation state.

(21) Kalz, W.; Homborg, H.; Kuppers, H.; Kennedy, B. J.; Murray, K. S. *Z. Naturforsch* **1984**, *39B*, 1478.
(22) Kennedy, B. J.; Murray, K. S.; Zwack, P. R.; Homborg, H.; Kalz, W. *Inorg. Chem.* **1986**, *25*, 2539−2545.
(23) Stymne, B.; Sauvage, F. X.; Wettermark, G. *Spectrochim. Acta* **1980**, *36A*, 397−402.
(24) Lever, A. B. P.; Wilshire, J. P. *Inorg. Chem.* **1978**, *17*, 1145−1151.
(25) Kobayashi, N.; Koshiyama, M.; Funayama, K.; Osa, T.; Shirai, H.; Hanabusa, K. *J. Chem. Soc., Chem. Commun.* **1983**, 913−914.
(26) Kobayashi, N.; Funayama, K.; Koshiyama, M.; Osa, T.; Shirai, H.; Hanabusa, K. *J. Chem. Soc., Chem. Commun.* **1983**, 915−916.
(27) Lever, A. B. P.; Minor, P. C.; Wilshire, J. P. *Inorg. Chem.* **1981**, *20*, 2550.
(28) Nicholson, R. S.; Shain, I. *Anal. Chem.* **1964**, *36*, 706.

Table 1. Band-Fitting Parameters[a] for Na[$(CN)_2Fe^{III}Pc(-2)$] in 70:30 DCM:CB

band no.	ν/cm^{-1}	λ/nm	$\Delta\nu$/cm^{-1}	D_0[b]	band type	$\langle\Delta\epsilon_M\rangle_0$[c]	C_0, B_0[d]/10^{-3}	(B_0, C_0)/D_0
1	12508	799	240	0.147	C	3.238	21.23	0.144
2	12820	780	218	0.259	C	27.20	178.4	0.689
3	13135	761	578	0.490	C	24.41	160.0	0.327
4	13617	734	482	0.395	C	−3.197	20.96	−0.053
5	14041	712	321	0.779	C	9.808	64.31	0.083
6	14349	697	273	2.535	C	−16.16	−106.0	
7	14578	686	214	6.884	C	130.8	857.3	0.125
8	14804	675	386	1.632	C	61.86	405.6	0.249
9	15080	663	468	2.696	C	30.91	202.6	0.075
10	15505	645	361	2.929	C	−238.7	−1566.0	−0.534
11	15750	635	535	1.615	C	−125.5	−823.3	−0.510
12	16069	622	436	1.799	C	−0.638	−4.181	−0.002
13	16314	613	350	0.978	C	−63.84	−418.6	−0.428
14	16641	601	420	1.587	C	−118.7	−778.6	−0.491
15	16982	589	356	0.584	C	−16.64	−109.1	−0.187
16	17298	578	578	1.156	C	−64.13	−420.6	−0.364
17	17781	562	585	1.864	C	−12.44	−81.62	−0.044
18	18179	550	429	1.141	C	38.05	249.5	0.219
19	18479	541	475	1.802	C	60.32	395.6	0.220
20	18906	529	534	1.022	C	18.89	123.8	0.121
21	19505	513	1021	2.117	C	66.45	435.7	0.206
22	20382	491	939	1.206	C	37.06	243.0	0.201
23	20939	478	832	0.411	C	−3.731	−244.6	−0.595
24	21574	464	1174	1.405	C	−13.45	−88.15	−0.063
25	22483	445	883	1.016	C	16.69	109.5	0.108
26	23313	429	869	1.224	C	37.53	246.1	0.201
27	23764	421	707	2.106	C	−19.21	−126.0	−0.060
28	24546	407	1034	3.449	C	−33.27	−218.2	−0.063
29	25349	394	1063	3.040	C	−30.77	−201.8	−0.066
30	26292	380	1325	3.356	C	22.18	145.5	0.043
31	27586	363	1621	4.975	C	−18.68	−122.6	−0.025
32	28912	346	1299	5.313	C	138.3	906.5	0.171
33	30187	331	1592	7.192	C	−35.33	−231.6	−0.032
34	31572	317	2072	10.19	C	−342.2	−2244.0	−0.220
35	33534	298	2138	6.538	C	−135.7	−889.6	−0.136
36	35156	284	1967	4.577	C	−42.07	−275.9	−0.060
37	36649	273	2180	7.834	C	121.0	793.6	0.094
38	38513	260	1568	4.924	C	18.39	120.6	0.024
39	40255	248	2082	10.65	C	6.299	41.30	0.004

[a] Statistics. B region: $\lambda_{245-520\ nm}$, $\chi^2 = 48.16$, $\Sigma(\Delta\epsilon)^2 = 2.36 \times 10^6$. Q region: $\lambda_{470-800\ nm}$, $\chi^2 = 133.1$, $\Sigma(\Delta\epsilon)^2 = 8.09 \times 10^6$. [b] $D_0 = \langle\epsilon\rangle_0/326.6$, where the units of D_0 (dipole strength) are D^2 (Debye units).[25] [c] $\langle\Delta\epsilon_M\rangle_0$ is the zeroth moment of the MCD. When fit with B and C terms the program calculates $\langle\Delta\epsilon_M\rangle_0$. [d] The Faraday term values, C_0 and B_0, are calculated directly from the moments as follows: B_0, $C_0 = \langle\Delta\epsilon_M\rangle_0$.

The absorption spectrum reported for five coordinate pyridinoiron(II) phthalocyanine[23] has a spectral envelope consistent with the III, not the II oxidation state of the iron. Exchange of an axial pyridine ligand with free chloride in the chlorinated solvent results in a negative shift in the E value of the Fe(II)/Fe(III) couple and a spontaneous metal oxidation. Oxidation of the iron core in $Na_2[(CN)_2Fe^{II}Pc(-2)]$ behaves slightly differently from the above examples. The crystal structure of $[PNP][(CN)_2Fe^{III}Pc(-2)]$ (PNP = bis(triphenylphosphine)nitrogen(1+)[29] demonstrates that both axial cyanide ligands are retained when iron is oxidized to the iron(III) state. This behavior is due to the negative charge on cyanide which results in it acting both as a counterion and a basic ligand.

Assignment of the Electronic Ground State in Na[$(CN)_2Fe^{III}Pc(-2)$]. Although there are a variety of absorption spectra reported for $L(X)Fe^{III}Pc(-2)$ complexes,[10,21-24] very few MCD spectra are available.[1,2] With the lack of available MCD spectra, the results obtained for the isoelectronic manganese(II) phthalocyanine ($Mn^{II}Pc(-2)$)[4,10,30] species are useful in the analysis of the MCD spectra reported here for $Na[(CN)_2Fe^{III}Pc(-2)]$.

Low ($S = {}^1/_2$) or intermediate ($S = {}^3/_2$) spin states are possible for the E_g ground state of the iron(III) ion. Analysis of low temperature, matrix-isolated MCD spectra of $Mn^{II}Pc(-2)$[30] showed that the ground state was $^4E_g(e_g{}^3b_{2g}a_{1g})$. The spin state for $Na[(CN)_2Fe^{III}Pc(-2)]$ may differ from intermediate spin ($S = {}^3/_2$) $Mn^{II}Pc(-2)$ because of the different conditions that the MCD spectra were measured under. Spectral measurements on $Mn^{II}Pc(-2)$ were performed in an argon matrix where the manganese ion is square planar, while the measurements on $[Fe^{III}Pc(-2)]^+$ were performed on low temperature glasses where the iron(III) ion is expected to be octahedrally coordinated. The crystal structure of $[PNP][(CN)_2Fe^{III}Pc(-2)]$[29] confirms the octahedral structure of the $[(CN)_2Fe^{III}Pc(-2)]^-$ anion. The iron(III) ion is located in the plane of the Pc(−2) ring, with axial Fe−C and equatorial Fe−N bond distances of 1.90 and 1.941 Å, respectively.

The different structural arrangements in $Na[(CN)_2Fe^{III}Pc(-2)]$ and $Mn^{II}Pc(-2)$ will affect the location and the energies of the 3d orbitals. The influence of octahedral (O_h) and tetragonal (D_{4h}) fields on the metal 3d shell are illustrated in Figure 7A. The positioning of the orbitals under a weak tetragonal field is the accepted order for low spin $L_2Fe^{II}Pc(-2)$ complexes.[31-33] The assignment of the $^4E_g(e_g{}^3b_{2g}a_{1g})$ ground state to Mn(II)Pc(−2) indicates a crossover in the e_g and the

(29) Kuppers, H.; Kalz, W.; Homborg, H. *Acta Crystallogr., Sect. C: Cryst. Struct. Commun.* **1985**, *C41*, 1420−1423.
(30) Williamson, B. E.; VanCott, T. C.; Boyle, M. E.; Misener, G. C.; Stillman, M. J.; Schatz, P. N. *J. Am. Chem. Soc.* **1992**, *114*, 2412−2419.
(31) Jones, J. G.; Twigg, M. V. *Inorg. Chem.* **1969**, *8*, 2120−2123.
(32) Sweigart, D. W. *J. Chem. Soc., Dalton Trans.* **1976**, 1476−1477.

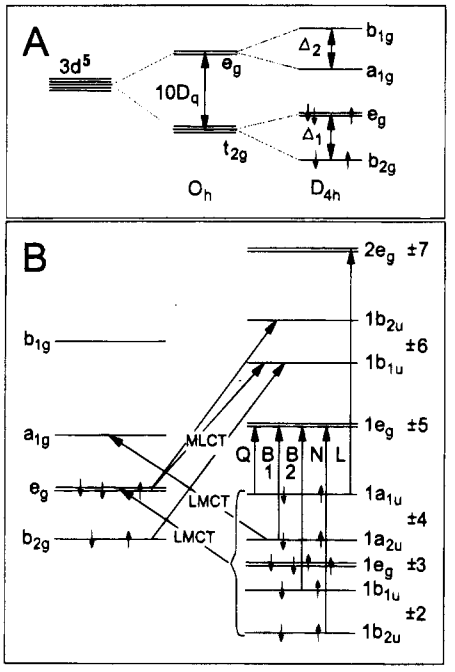

Figure 7. (A) Energy level splitting for metal 3d orbitals under a ligand field with octahedral ($10Dq$) and axial (Δ_1,Δ_2) distortions. (B) Selected molecular orbitals for the ^2E_g ground state of low spin ($S = {}^1/_2$) [Fe^{III}-$Pc(-2)]^+$.

b_{2g} orbital energies, shown in Figure 7A, under the strong tetragonal distortion expected for a square planar complex. The iron(III) ion in $Na[(CN)_2Fe^{III}Pc(-2)]$ is expected to retain the orbital arrangement featured in Figure 7A, due to the weak tetragonal distortion. The two lowest lying orbitally degenerate spin states available for $Na[(CN)_2Fe^{III}Pc(-2)]$ are $^2E_g(b_{2g}^2e_g^3)$ and $^4E_g(b_{2g}^2e_ga_{1g}b_{1g})$. The energy separation between the e_g, and the a_{1g} and b_{1g} orbitals is not expected to vary significantly between low spin $Na_2[(CN)_2Fe^{II}Pc(-2)]$[34] and $Na[(CN)_2Fe^{III}$-$Pc(-2)]$; therefore the ground state is assigned as low spin ^2E_g-$(b_{2g}^2e_g^3)$. The g_{av} factor of 4.6 for $Na[(CN)_2Fe^{III}Pc(-2)]$, obtained from low temperature MCD spectral analysis, and the $g_{\parallel} = 2.03$ and $g_{\perp} = 1.87$ values from the EPR spectra of iron-(III) tetracarbonylphthalocyanine[25] are also consistent with a low spin ($S = {}^1/_2$) ^2E_g ground state. We should note that Kennedy et al.[22] report that for the dicyano complex, $[(CN)_2$-$Fe^{III}Pc(-2)$, the EPR bands were very broad and indistinct; we also have determined that the EPR signal for this compound is poorly resolved, broadening as the temperature falls (unpublished data).

Allowed Electronic Transitions for Low Spin ($S = {}^1/_2$) $Fe^{III}Pc(-2)$. Specific transitions within the molecular orbitals of the 18-π-electron system of the $Pc(-2)$ ring and the iron-(III) 3d orbitals are illustrated in Figure 7B. In addition to the major ring based transitions, the Q, B1, B2, N, and L bands, there are a significant number of allowed LMCT and MLCT transitions. The allowed CT transitions, the direction of CT, and the transition polarization are listed in Table 2.

Depending on the transition polarization, two distinct types of C terms will contribute to the MCD spectral envelopes. An xy (E_u) polarized transition, which arises from a transition from a degenerate ground state into a nondegenerate excited state, is displayed in Figure 8A. The $Pc(-2)$ ring, the two MLCT, and several LMCT transitions are polarized in the xy direction. In the presence of spin–orbit coupling (H_{so}), the ^2E_g ground state

(33) Watkins, J. J.; Balch, A. L. *Inorg. Chem.* **1975**, *14*, 2720–2723.
(34) Ough, E. A.; Stillman, M. J. Submitted for publication.

Table 2. Allowed Charge Transfer Transitions for Low Spin ($S = {}^1/_2$) $[Fe^{III}Pc(-2)]^+$ [a]

one electron transition	excited state[c]	charge transfer	polarization of transition	MCD term expected[b]
$a_{1u}, a_{2u} \rightarrow a_{1g}, b_{1g}$	^2E_u	L → M	z	C_B
$b_{1u}, b_{2u} \rightarrow a_{1g}, b_{1g}$	^2E_u	L → M	z	C_B
$a_{1u} \rightarrow e_g$	$^2A_{1u}$	L → M	xy	C_A
$a_{2u} \rightarrow e_g$	$^2A_{2u}$	L → M	xy	C_A
$b_{1u} \rightarrow e_g$	$^2B_{1u}$	L → M	xy	C_A
$b_{2u} \rightarrow e_g$	$^2B_{2u}$	L → M	xy	C_A
$b_{1g} \rightarrow b_{1u}, b_{2u}$	^2E_u	M → L	z	C_B
$e_g \rightarrow b_{1u}$	$^2A_{iu}, {}^2B_{iu}$	M → L	xy	C_A
$e_g \rightarrow b_{2u}$	$^2A_{iu}, {}^2B_{iu}$	M → L	xy	C_A

[a] The ground state electronic configuration of the iron 3d orbitals is $(b_{2g})^2(e_g)^3$ and the symmetry of the ground state is ^2E_g. [b] The subscripts A and B denote that the transitions are xy and z polarized, respectively.

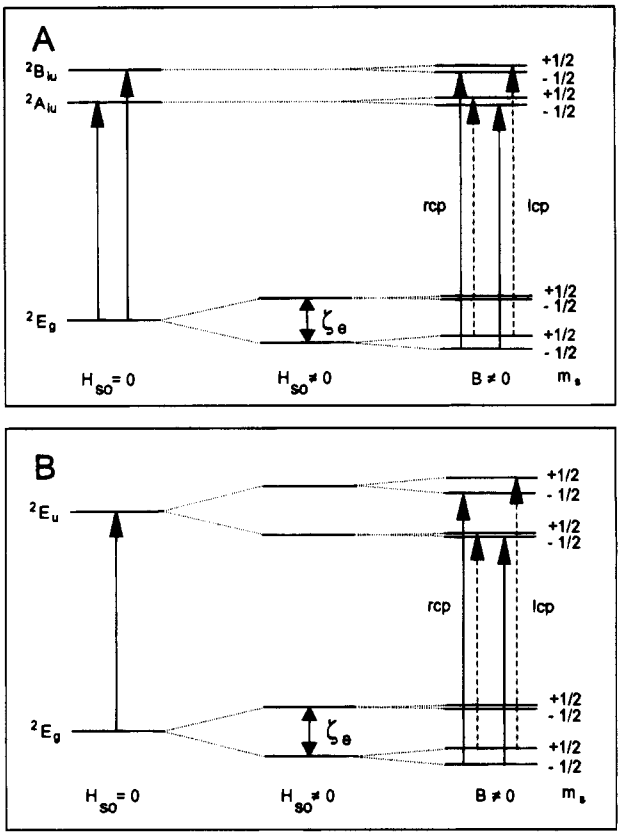

Figure 8. Energy level diagrams for (A) the $^2E_g \rightarrow {}^2A_{iu}, {}^2B_{iu}$ ($i = 1, 2$) transitions and (B) the $^2E_g \rightarrow {}^2E_u$ transitions. The Zeeman ($H_{so} \neq 0$) and the spin–orbit (ζ_e) splittings are highly exaggerated with respect to the energy separation between electronic states. Right circularly polarized (rcp) and left circularly polarized (lcp) transitions for the lowest energy ground state Kramers doublet are plotted. The solid arrows represents the transitions expected when the MCD signal saturates, while the dashed arrows represent the additional transition that occur when the MCD signal is not saturated.

is split into two Kramers doublets. For an applied magnetic field ($\mathbf{B} \neq 0$), the solid arrows in Figure 8A, represents the only allowed transitions when the ground state is saturated. The difference in the ground and excited state magnetic moments will determine the sign (+) or (−) of the MCD signal arising from each transition. The xy-polarized C terms are denoted as C_A terms, where the A subscript denotes the xy degeneracy in the transition polarization.

If both the ground and excited states are orbitally degenerate, as shown in Figure 8B, then the electronic transition is z (A_{2u}) polarized. Several LMCT and MLCT transitions listed in Table 2 are polarized in the z direction. Because spin–orbit coupling

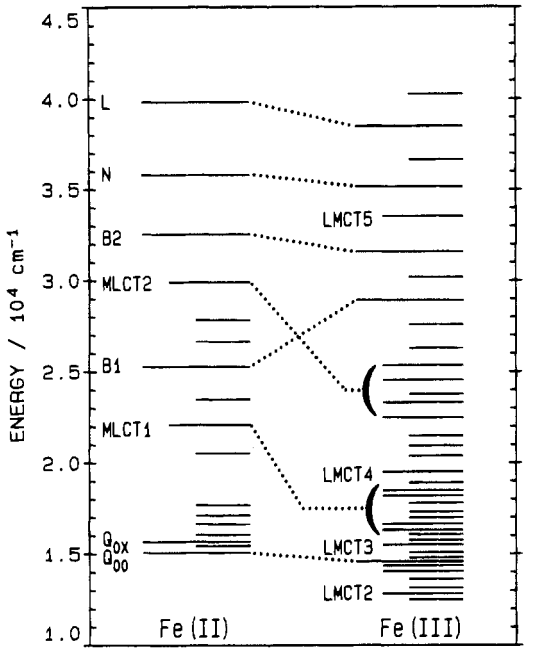

Figure 9. Comparison of the fitted band center energies for Na[$(CN)_2Fe^{III}Pc(-2)$] and $Na_2[(CN)_2Fe^{II}Pc(-2)]$.[34] The line lengths are: long for Pc(−2) transitions, intermediate for CT transitions and small for unassigned transitions.

Table 3. Assigned Transitions for the Absorption and MCD Spectra of Na[$(CN)_2Fe^{III}Pc(-2)$]

band	one electron transition	excited state	*C* term sign	λ/nm	ν/cm⁻¹
Q	$1a_{1u}(\pi) \rightarrow 1e_g(\pi^*)$	$^2A_{1u}$	+	686	14578
B1	$1a_{2u}(\pi) \rightarrow 1e_g(\pi^*)$	$^2A_{2u}$	+	346	28912
B2	$1b_{1u}(\pi) \rightarrow 1e_g(\pi^*)$	$^2B_{1u}$	−	317	31572
N	$2a_{2u}(\pi) \rightarrow 1e_g(\pi^*)$	$^2A_{2u}$	+	273	36649
L	$1a_{1u}(\pi) \rightarrow 2e_g(\pi^*)$	$^2A_{1u}$	+	260	38513
MLCT1	$e_g(d\pi) \rightarrow 1b_{1u}(\pi^*)$	$^2B_{iu}$	−	613	16314
		$^2B_{iu}$	−	601	16641
		$^2A_{iu}$	+	550	18179
		$^2A_{iu}$	+	541	18479
MLCT2	$e_g(d\pi) \rightarrow 1b_{2u}(\pi^*)$	$^2A_{iu}$	+	445	22483
		$^2A_{iu}$	+	429	23313
		$^2B_{iu}$	−	407	24546
		$^2B_{iu}$	−	394	25349
LMCT2	$1a_{2u}(\pi) \rightarrow e_g(d\pi)$	$^2A_{2u}$	+	780	12820
LMCT3	$1b_{1u}(\pi) \rightarrow e_g(d\pi)$	$^2B_{1u}$	−	645	15505
LMCT4	$1a_{2u}(\pi) \rightarrow e_g(d\pi)$	$^2A_{2u}$	+	513	19505
LMCT5	$1b_{2u}(\pi) \rightarrow e_g(d\pi)$	$^2B_{2u}$	−	298	33534
	$1a_{1u}(\pi) \rightarrow b_{1g}(d)$	^2E_u	−	712	14041
			+	697	14349

splits the ground and excited states into pairs of Kramers doublets, *z*-polarized transitions will consists of individual transitions into each excited state Kramers doublet. The matrix isolation study of $Mn^{II}Pc(-2)$[30] determined the spin−orbit coupling parameter (ζ) to be about 300 cm⁻¹. Since the Zeeman splittings (<10 cm⁻¹) are small compared to the spin−orbit splitting, ζ approximates the energy separation between the two transitions that comprise a *z*-polarized band. The two transitions occur as oppositely signed MCD C terms and are labelled C_{B+} and C_{B-}, with B denoting *z* polarization and the +/− labels indicating the sign of the MCD signal.

Assignment of the Low Temperature Absorption and MCD Spectral Fits. The deconvoluted fits presented here represent the first spectral deconvolution calculations reproted for an open shell metallophthalocyanine with a degenerate ground state. The large number of bands (39) required to fit the 250−900 nm region of the absorption (77 K) and MCD (4 K) spectra for Na[$(CN)_2Fe^{III}Pc(-2)$] makes the task of assigning

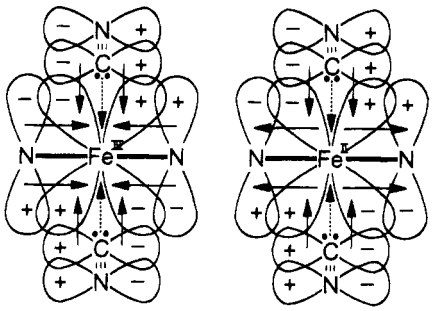

Figure 10. Selected overlapping iron (dπ) and ligand (π and π*) molecular orbitals in (A) Na[$(CN)_2Fe^{III}Pc(-2)$] and (B) $Na_2[(CN)_2Fe^{II}Pc(-2)]$.[13] The arrows represent the direction of electron donation.

specific bands to ring ($\pi \rightarrow \pi^*$), MLCT ($d \rightarrow \pi$), and LMCT ($\pi \rightarrow d$) transitions difficult. The spectral fits for $L_2MgPc(-2)$,[8] $LZnPc(-2)$,[10] and $L_2Fe^{II}Pc(-2)$[34] are invaluable in the identification of the $\pi \rightarrow \pi^*$ and the MLCT transitions. The fitted band center energies for $Na_2[(CN)_2Fe^{II}Pc(-2)]$[34] and Na[$(CN)_2Fe^{III}Pc(-2)$] are displayed in Figure 9, while the spectral assignments from the absorption and MCD spectra of Na[$(CN)_2Fe^{III}Pc(-2)$] are summarized in Table 3.

The Q, B1, B2, N, and L Bands. The absorption band centered at 686 nm (14 578 cm⁻¹) is assigned as the Q band. The B1, B2, N, and L bands are difficult to locate because CT bands overlap and camouflage their exact locations within the spectral envelopes. The positions of these four transitions can be determined by understanding the effect of iron(III) on the Pc(−2) π and π* orbitals and by predicting the sign (+ or −) of the MCD C_A terms. The removal of an $e_g(d\pi)$ electron to form the Fe(III) results in electron deficiency at the iron core, which is partially compensated for by the removal of electron density from the axial CN^- and equatorial Pc(−2) ligands, as shown in Figure 10A (the example for *iron(II)* in $Na_2[(CN)_2Fe^{II}Pc(-2)]$ is illustrated in Figure 10B). Results from $L_2Fe^{II}Pc(-2)$ indicate that the π-donor/π-acceptor properties of the Pc(−2) ring are very much chameleon-like and a shift from π acceptor to π donor upon oxidation to iron(III) is not unexpected.[13] The spectral changes due to the withdrawal of π electron density from the Pc(−2) ring are expected to resemble those observed in phthalocyanine π-cation radicals[2,7,9,10] and those observed in $(NH_3)(CO)Fe^{II}Pc(-2)$,[34] where the strong π acceptor carbon monoxide (CO) ligand pulls electron density away from the Pc(−2) ring. Employing the $[MgPc(-1)]^{\bullet+}$ [2,9] and $(NH_3)(CO)Fe^{II}Pc(-2)$[34] fits as templates, the following changes are expected upon oxidation from $Na_2[(CN)_2Fe^{II}Pc(-2)]$ to Na[$(CN)_2Fe^{III}Pc(-2)$]: the energy separation between the B1/B2 band pairs will be reduced; changes in the energies of th B2, N, and L bands will be small; and the B1 band is expected to be blue shifted.

For a ^2E_g ground state, the symmetries of the ground and excited state determine the sign of the MCD C_A terms.[19,30] The transitions with $^2A_{1u}$ (Q and L) and $^2A_{2u}$ (B1 and L) excited state symmetries have C_A terms whose signs are opposite to those transitions with $^2B_{1u}$ (B2) and $^2B_{2u}$ excited state symmetries. Our assignment of the (+) MCD C_A term at 686 nm (14 578 cm⁻¹) as Q requires the B1, N, and L transitions to appear as (+) C_A terms and requires the B2 band to appear as a (−) C_A term. The bands centered at 346 nm (28 912 cm⁻¹) (+), 317 nm (31 572 cm⁻¹) (−), 273 nm (36 649 cm⁻¹) (+) and 260 nm (38 513 cm⁻¹) (+) are assigned to B1, B2, N, and L, respectively. This assignment is consistent with the expected

changes in the transition energies following metal oxidation and with the predicted signs of the MCD C terms.

Degenerate Charge Transfer Bands. The information presented in Figure 7 and Table 2 suggests that seven CT transitions appear as MCD C_A terms. Since the $e_g(d\pi) \rightarrow \{1b_{1u}(\pi^*),1b_{2u}(\pi^*)\}$ (MLCT1 and MLCT2) transitions each split into four excited states with $^2A_{1u}$, $^2A_{2u}$, $^2B_{1u}$ and $^2B_{2u}$ symmetries,[30] the associated MCD signals will consist of sets of four C_A terms. The five allowed LMCT transitions $\{1a_{1u}(\pi),1a_{2u}(\pi),1b_{1u}(\pi),2a_{2u}(\pi),1b_{2u}(\pi)\} \rightarrow e_g(d\pi)$ (LMCT1−5) have excited state symmetries of $^2A_{1u}$, $^2A_{2u}$, $^2B_{1u}$, $^2A_{2u}$ and $^2B_{2u}$ and the signs of the corresponding C_A terms will be (+), (+), (−), (+), and (−), respectively.

In the study by Lever et al.[4] transition energies were correlated with the oxidation and reduction potentials for the isoelectronic $Mn^{II}Pc(-2)$ molecule. The $e_g(d\pi) \rightarrow 1b_{1u}(\pi^*)$ (MLCT1) electronic transition was predicted to lie near 635 nm (15 725 cm^{-1}). Because there are no reported values for the $Fe^{III}Pc(-1)/Fe^{IV}Pc(-1)$ oxidation couple, the electrochemical measurements alone cannot be used to predict the location of MLCT1 in $Na[(CN)_2Fe^{III}Pc(-2)]$. To minimize any confusion we note here that our labeling of CT differs from Lever et al.[4] in that they assigned the parity-forbidden $e_g(d\pi) \rightarrow e_g(\pi^*)$ transition as MLCT1 and the allowed $e_g(d\pi) \rightarrow 1b_{1u}(\pi^*)$ transition as MLCT2, while we assign the two allowed $e_g(d\pi) \rightarrow 1b_{1u}(\pi^*)$ and $e_g(d\pi) \rightarrow 1b_{2u}(\pi^*)$ transitions as MLCT1 and MLCT2, respectively. Considering the influence of configuration interaction, which is not included in Lever's method,[4] the locations of the four transitions at 613 nm (16 314 cm^{-1}) (−), 601 nm (16 641 cm^{-1}) (−), 550 nm (18 179 cm^{-1}) (+), and 541 nm (18 479 cm^{-1}) (+) are comparable with the predicted location of MLCT1 at 635 nm in $Mn^{II}Pc(-2)$.[4,30] The presence of two (+) and two (−) intensity C_A terms is consistent with the assignment of these bands to the MLCT1 series. On the basis of the blue shift in the MLCT1 band center following metal oxidation and the previous location of MLCT2 in $Na_2[(CN)_2Fe^{II}Pc(-2)]$, the MLCT2 series in $Na[(CN)_2Fe^{III}Pc(-2)]$ is expected to be centered around 400 nm. The four C_A terms at 445 nm (22 483 cm^{-1}) (+), 429 nm (23 313 cm^{-1}) (+), 407 nm, (24 546 cm^{-1}) (−), and 394 nm (25 349 cm^{-1}) (−) are in the appropriate region, have the appropriate MCD band intensities, and are assigned as MLCT2 bands.

The transition responsible for the (+) intensity MCD C_A term at 780 nm (12 820 cm^{-1}) is either LMCT1 or LMCT2. The predicted locations of the LMCT1 and LMCT2 bands for $Mn^{II}Pc(-2)$[4,30] are 911 nm (10 970 cm^{-1}) and 381 nm (26 180 cm^{-1}), respectively, and based on the reported oxidation and reduction potentials for $Na_2[(CN)_2Fe^{II}Pc(-2)]$[3] are 1097 nm (9113 cm^{-1}) (LMCT1) and 426 nm (23 447 cm^{-1}) (LMCT2) for $Na[(CN)_2Fe^{III}Pc(-2)]$. On the basis of the above results, the 780 nm band should be assigned as LMCT1, but this assignment is not consistent with the reported absorption spectrum for low spin iron(III) tetracarbonylphthalocyanine,[25] which shows the presence of two weak CT bands at 1100 and 1200 nm. If the 780 nm band is LMCT1, then these CT bands should not be present because CT bands with energies lower than LMCT1 are not expected. As stated earlier, the major difficulty in correlating transition energies with oxidation and reduction potentials is that effects due to configuration interaction are not taken into account. The spectral results indicate that configuration interaction does have a significant influence on the energies of the MLCT transitions, and therefore the 780 nm band is assigned as LMCT2.

The 500−690 nm MCD spectral region is difficult to interpret because in addition to the Q_{00} and Q_{vib} bands, which typically

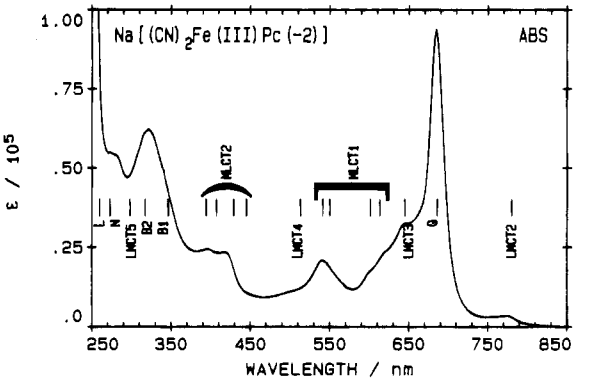

Figure 11. Room temperature (300 K) absorption spectra of $Na[(CN)_2Fe^{III}Pc(-2)]$ in DCM. The location of the assigned $\pi \rightarrow \pi^*$, MLCT, and LMCT band centers, which were obtained from deconvolution of the low temperature spectra, are represented by the labeled vertical lines.

extend across a 3000 cm^{-1} [1] energy range in metallophthalocyanines, LMCT bands are also expected. Ignoring configuration interaction, the 2600 cm^{-1} gap between the B1 and B2 bands and the location of LMCT2 at 780 nm suggest that LMCT3 will overlap the Q_{vib} manifold around 650 nm (15 385 cm^{-1}). The intense (−) intensity MCD C_A term at 645 nm (15 505 cm^{-1}) is in the appropriate location, has the correct sign, and is assigned as LMCT3. The large C_0/D_0 ratio (−0.534; Table 1) for LMCT3 may be attributed to intensity borrowing from the Q_{vib} manifold. The LMCT4 band is expected around 520 nm and is assigned to the (+) MCD C_A term at 513 nm (19 505 cm^{-1}). The energy separation (approximately 13 500 cm^{-1}) between the N and C bands, based on the general location of the C band, in the vapor phase absorption spectra of various metallophthalocyanines,[35] at 200 nm (50 000 cm^{-1}), approximates the energy separation between LMCT4 and LMCT5 and places LMCT5 near 300 nm (33 333 cm^{-1}). The (−) C_A term at 298 nm (33 534 cm^{-1}) is assigned as LMCT5.

Nondegenerate Charge Transfer Bands. Although Table 2 lists several *z*-polarized CT transitions, only one set of C_B terms was isolated from the MCD spectrum of $Na[(CN)_2Fe^{III}Pc(-2)]$. The oppositely signed *C* terms at 697 nm (14 349 cm^{-1}) (+) and 712 nm (14 041 cm^{-1}) (−) are separated by 308 cm^{-1}, a value which matches the spin−orbit coupling parameter (ζ). These two bands are MCD C_{B+} and C_{B-} terms and based on their energies they represent either the $1a_{1u}(\pi) \rightarrow a_{1g}(d^*)$ or $1a_{1u}(\pi) \rightarrow b_{1g}(d^*)$ transition. We believe that the absorption bands reported at 1100 and 1200 nm for iron(III) tetracarbonylphthalocyanine[25] represent the spin−orbit split components of the $1a_{1u}(\pi) \rightarrow a_{1g}(d^*)$ transition; therefore, the 697 and 712 nm bands are assigned to the $1a_{1u}(\pi) \rightarrow b_{1g}(d^*)$ transition.

Comparison of the $Na[(CN)_2Fe^{III}Pc(-2)]$ and $Na_2[(CN)_2Fe^{II}Pc(-2)]$ [X] Spectral Fits. The spectral differences between low spin ($S = 0$) $Na_2[(CN)_2Fe^{II}Pc(-2)]$ and low spin ($S = {}^1/_2$) $Na[(CN)_2Fe^{III}Pc(-2)]$ arise from the removal of an iron $e_g(d\pi)$ electron. In addition to "new" CT transitions into the $^3/_4$-filled $e_g(d\pi)$ orbitals, *z*-polarized transitions, which are formally forbidden under the $^1A_{1g}$ ground state symmetry of $Na_2[(CN)_2Fe^{II}Pc(-2)]$, become allowed under the ^2E_g ground state symmetry of $Na[(CN)_2Fe^{III}Pc(-2)]$. The increase in the number of fitted bands upon metal oxidation, as shown in Figure 9, demonstrates the increased CT contribution to the spectral envelope of $Na[(CN)_2Fe^{III}Pc(-2)]$.

An increase in the number of CT transitions is not the only different in the spectra of $Na_2[(CN)_2Fe^{II}Pc(-2)]$ and Na-

(35) Edwards, L.; Gouterman, M. *J. Mol. Spectrosc.* **1970**, *33*, 292−310.
(36) Upton, A. H. P.; Williamson, J. *Phys. Chem.* **1994**, *98*, 71−76.

$[(CN)_2Fe^{III}Pc(-2)]$. There are also significant changes in the energies of the Q, B1, MLCT1, and MLCT2 transitions. Metal oxidation effects a change in the direction of π donation between the iron core and the Pc(−2) ring. With the vacancy in the $e_g(d\pi)$ orbitals, iron now pulls electron density away from the Pc(−2) ring. This explains the compression of the B1/B2 band pair, a spectral feature which is common in $L(CO)Fe^{II}Pc(-2)$, where CO, a strong π acceptor ligand, pulls electron density away from the Pc(−2) ring.[34]

Conclusions

Low temperature (4 K), variable field (0−4 T) MCD spectra of metal oxidized $Na[(CN)_2Fe^{III}Pc(-2)]$ were employed in the assignment of the ^2E_g ground state to this molecule. The average orbital g_{av} factor of 4.6 ± 0.04 for $Na[(CN)_2Fe^{III}Pc(-2)]$ was determined from the field dependence studies. Low temperature absorption (77 K) and MCD (4 K) spectra were subjected to spectral deconvolution calculations to determine the energies of Pc(−2) ring, LMCT and MLCT transitions. The complete spectral analysis for $Na[(CN)_2Fe^{III}Pc(-2)]$ has been summarized in the absorption spectrum shown in Figure 11.

Acknowledgment. We gratefully acknowledge funding from the Natural Sciences and Engineering Research Council of Canada. M.J.S. is a member of the Centre for Chemical Physics and the Photochemistry Unit at the University of Western Ontario. This is publication 517 of the Photochemistry Unit.

IC940522D